New Optical Waveguide Design Based on Wavefront Matching Method

Yohei Sakamaki, *Member, IEEE*, Takashi Saida, *Member, IEEE*, Toshikazu Hashimoto, and Hiroshi Takahashi, *Member, IEEE*

***Abstract*—We have studied the wavefront matching (WFM) method, which synthesizes optimum waveguide patterns from the desired characteristics, and demonstrated its feasibility. In this paper, we expand this method to create optimum waveguide shapes with low-loss and low-wavelength dependence in waveguide lenses, Y-branches, and waveguide crossings. We describe the design procedures for each waveguide element and report the experimental results as proof of concept. The measured results agree well with our design requirements, and the waveguide patterns designed by the WFM method exhibit better characteristics than the reference patterns.**

***Index Terms*—Design methodology, optical planar waveguides.**

I. Introduction

SILICA-BASED planar lightwave circuit (PLC) devices, including arrayed waveguide grating multiplexers/demultiplexers, thermo-optic switches, variable optical attenuators, and splitters, are now widely used in both access and backbone networks owing to their mass producibility, long-term reliability, and good optical characteristics [1]. As their use has spread, requirements that are related to performance improvement and miniaturization of the PLC devices have become stricter with a view to constructing higher capacity, more flexible, and lower cost optical communication systems. To overcome the performance limitation of the conventional PLC devices, extensive studies have been undertaken to develop new ways of optimizing waveguide patterns [2]–[6]. For instance, a genetic algorithm has been recently applied to the design of very short spot-size converters [2], [5] and polarization rotators [4]. However, its use is solely limited to simple devices because it is a cut-and-try approach that requires a long calculation time and a large amount of computer memory.

In contrast, Hashimoto *et al.* [7] proposed the wavefront matching (WFM) method, which enables us to deterministically synthesize an optimum refractive-index distribution (a waveguide pattern) in optical circuits from the desired characteristics. Therefore, the WFM method requires less calculation time than the cut-and-try algorithm method and creates a waveguide pattern that is beyond our imagination. A very compact wavelength demultiplexer with a mosaic-like pattern composed of core and cladding pixels has already been successfully demonstrated with the WFM method [8]. Since the light scattering and interference induced by the mosaic-like pattern are actively used to obtain large wavelength dependence, the circuit size is very compact compared with a conventional Mach–Zehnder type filter. However, the 2-D array of core and cladding pixels causes light scattering in a direction perpendicular to the substrate, and this yields excess loss. With regard to a silica-based PLC with a low refractive-index difference, the loss is very large since the pixel size is limited to a few micrometers due to the limited aspect ratio of the etching process.

To achieve our second aim, namely, to optimize existing waveguide elements such as Y-branches and waveguide crossings, we propose a new design approach based on the WFM method, which we call the "solid pattern" approach. In the calculation procedure used for the WFM method, we avoid placing cladding in a pixel surrounded by core pixels, and this results in a solid rather than a mottled pattern. Compared with the original WFM method (which we call the "mosaic-like pattern" approach in this paper), this restriction can provide optimum waveguides with lower loss and less wavelength dependence because the vertical scattering and interference are suppressed in the solid pattern. In addition, the solid pattern clearly has better manufacturability than the mosaic-like pattern.

In this paper, we first describe the principle, namely, the common aspects of the mosaic and solid pattern approaches, of the WFM method. Then, we explain the design procedure of the solid pattern approach and compare it with the mosaic-like pattern approach by using waveguide lens design as an example. In addition, we demonstrate several waveguide elements designed with the solid pattern WFM method, including Y-branches [9] and waveguide crossings [10], which have lower excess losses than our reference branch and crossing patterns drawn with lines, to verify the practical effectiveness of our proposed approach.

II. Principle of the WFM Method

First, we describe a principle of the WFM method with a view to optimizing the waveguide patterns. For simplicity, we consider a slab waveguide with one input and one output port, as shown in Fig. 1. Our goal is to synthesize a waveguide pattern that guides the input light to the output port. Here, the input light propagates in the z-direction, and the waveguide is on the x–z plane. The y-direction is omitted because we use a 2-D model for simplicity. We define $\phi_0(x)$ as the input light field and $\psi_M(x)$ as the desired output field, where x is the lateral coordinate, and the subscripts 0 and M denote the calculation step number in the z-direction. The region to be

Manuscript received April 17, 2007; revised July 2, 2007.

The authors are with Nippon Telegraph and Telephone (NTT) Photonics Laboratories, NTT Corporation, Atsugi 243-0198, Japan (e-mail: sakamaki@aecl.ntt.co.jp).

Digital Object Identifier 10.1109/JLT.2007.906798

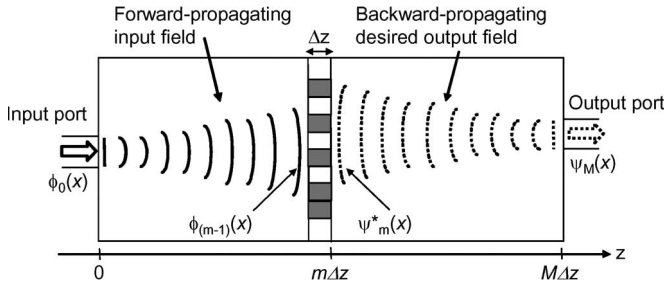

Fig. 1. Principle of WFM method.

optimized is divided into small pixels in steps of Δz and Δx in the z- and x-directions, respectively, and each pixel consists of a square of core or cladding material. Based on the above definition, the coupling efficiency between the output field from the optimized region and the desired output field needs to be unity. The coupling coefficient η is given by the overlap integral between the output field $\phi_M(x)$ and the desired output field $\psi_M(x)$, which is written as

$$\eta = \left| \int \psi_M^*(x)\phi_M(x)dx \right|^2. \tag{1}$$

According to the beam propagation method (BPM), the output field $\phi_M(x)$ is given by

$$\phi_M(x) = (\mathbf{AB}_M\mathbf{A})\cdots(\mathbf{AB}_m\mathbf{A})\cdots(\mathbf{AB}_1\mathbf{A})\phi_0(x) \tag{2}$$

where $\mathbf{A}$ is the operator for free space propagation, and $\mathbf{B}_m$ is the phase shift operator expressed as $\mathbf{B}_m(x) = \exp[-jk(n_m(x) - n_{\mathrm{ref}})\Delta z]$. k is the wavenumber of light, n_{ref} is the reference refractive index, and $n_m(x)$ is the refractive-index distribution at $z = m\Delta z$. From (1) and (2), the coupling coefficient η is written as

$$\eta = \left| \int \psi_M^*(x)\mathbf{AB}_M\mathbf{A}\cdots(\mathbf{AB}_m\mathbf{A})\cdots\mathbf{AB}_1\mathbf{A}\phi_0(x)dx \right|^2. \tag{3}$$

Here, let us consider a physical meaning of (3). The right side of $(\mathbf{AB}_m\mathbf{A})$, that is, $(\mathbf{AB}_{m-1}\mathbf{A})\cdots(\mathbf{AB}_1\mathbf{A})\phi_0(x)$, corresponds to the optical field $\phi_{m-1}(x)$ that arrives at $z = (m-1)\Delta z$ from the input port. On the other hand, assuming the reciprocity of an optical circuit, the left side of $(\mathbf{AB}_m\mathbf{A})$, i.e., $\psi_M^*(x)(\mathbf{AB}_M\mathbf{A})\cdots(\mathbf{AB}_{m+1}\mathbf{A})$, is equivalent to the backward-propagating field $\psi_m^*(x)$ that arrives at $z = m\Delta z$ from the output port. (We mathematically explain the adequacy of our interpretation in the Appendix.) Thus, we can rewrite (3) as follows:

$$\eta = \left| \int \psi_m^*(x)\mathbf{AB}_m\mathbf{A}\phi_{m-1}(x)dx \right|^2. \tag{4}$$

Equation (4) means that the overlap integral between the forward-propagating input field and the backward-propagating desired output field at an arbitrary position provides the coupling coefficient of an optical circuit.

To obtain the optimum waveguide pattern, we need to find the refractive-index distribution that provides the maximum coupling coefficient η. Here, if we change the refractive-index distribution to $n_m(x) + \delta n_m(x)$, the phase shift operator $\mathbf{B}'_m$ is expressed as

$$\begin{aligned}\mathbf{B}'_m &= \exp\{-jk(n_m(x) + \delta n_m(x) - n_{\mathrm{ref}})\Delta z\} \\ &\cong \mathbf{B}_m(1 - jk\delta n_m(x)\Delta z)\end{aligned} \tag{5}$$

where we assume $k\delta n_m(x)\Delta z \ll 1$. The coupling coefficient η' is calculated from (4) and (5) as

$$\begin{aligned}\eta' &= \left| \int \psi_m^* AB_m(1 - jk\delta n_m(x)\Delta z)A\phi_{m-1}(x)dx \right|^2 \\ &\cong \eta + 2k\Delta z\sqrt{\eta}\int \mathrm{Im}[\psi_m^*(x)\phi_{m-1}(x)]\,\delta n_m(x)dx.\end{aligned} \tag{6}$$

Note that since η is not relevant to the phase of $\psi_M(x)$, the phase of $\psi_M(x)$ is adjusted so that the following mathematical expression has equality:

$$\int \psi_m^*\mathbf{AB}_m\mathbf{A}\phi_{m-1}dx = \int \overline{\psi_m^*\mathbf{AB}_m\mathbf{A}\phi_{m-1}}dx. \tag{7}$$

In addition, $O(\delta n_m(x)^2\Delta z^2)$ is ignored in (6). Equation (6) shows that the coupling efficiency is always improved by setting $\delta n_m(x)$ so that it is proportional to $\mathrm{Im}[\psi_m^*(x)\phi_{m-1}(x)]$. From a physical standpoint, this mathematical operation corresponds to matching the wavefronts of the backward-propagating desired output field $\psi_m^*(x)$ and the forward-propagating input field $\phi_{m-1}(x)$ by modifying the local refractive-index distribution $n_m(x)$. As the refractive index of usual PLC devices is binary (core or cladding), we insert the core material if $\mathrm{Im}[\psi_m^*(x)\phi_{m-1}(x)]$ is a positive number and remove the core material if it is negative. Since each pixel is determined as core or cladding according to the sign of $\mathrm{Im}[\psi_m^*(x)\phi_{m-1}(x)]$, the refractive-index distribution obtained with the WFM method has mosaic-like core patterns. The whole refractive-index distribution is optimized by scanning the optimization point $z = m\Delta z$ from $z = M\Delta z$ to $z = 0$. We first calculate the forward-propagating input field before the optimization and optimize the refractive-index distribution at $z = M\Delta z$. Then, we move the optimization point to $z = (M-1)\Delta z$ while calculating the backward-propagating desired output field $\psi_{M-1}^*(x)$. We repeat this procedure step by step until the optimization point reaches $z = 0$. In this case, we need only two BPM calculations for the optimization. Of course, the coupling efficiency can be further improved by repeating the procedure mentioned above. If the optimization procedure is repeated N times, we need a total of $N+1$ BPM calculations. Thus, we can optimize waveguide patterns without a large number of calculations, unlike other optimization methods based on cut-and-try approaches.

As described above, the WFM method deterministically synthesizes the optimum refractive-index distribution according to $\mathrm{Im}[\psi_m^*(x)\phi_{m-1}(x)]$. However, the mosaic-like patterns designed with the original WFM method induce vertical light scattering that leads to loss. Thus, we propose a new approach based on the WFM method for designing the solid patterns to suppress the vertical scattering. With the solid pattern approach, the

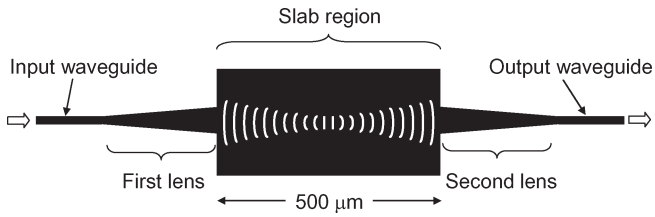

Fig. 2. Design layout of waveguide lens pair.

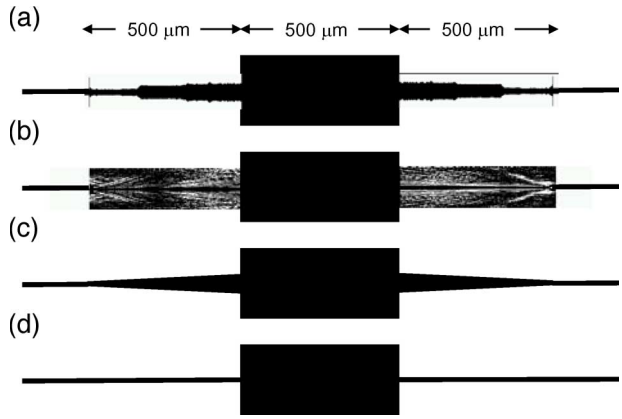

Fig. 3. Design waveguide pattern of lens pair. (a) Solid pattern approach. (b) Mosaic-like pattern approach. (c) Tapered waveguide. (d) Constant-width waveguide.

coupling efficiency is improved by modifying the waveguide width at $z = m\Delta z$ to match the wavefronts of $\psi_m^*(x)$ and $\phi_{m-1}(x)$. In Section III, we describe the effectiveness of the solid pattern approach in detail.

III. Solid Pattern Approach

In this section, we describe the solid pattern approach and compare it with the mosaic-like pattern approach by using the example of waveguide lens design. Then, we report the experimental results as proof of concept.

Here, we design waveguide lenses using the solid pattern approach and the mosaic-like pattern approach based on the WFM method. Fig. 2 illustrates this problem. The purpose of this design is to obtain the optimum waveguide lens shape to reduce the diffraction loss that occurs at a slab waveguide sandwiched between waveguide lens pairs that radiate converging beams, as shown in the figure. We place a 500-μm-long slab region between the two lenses. We use the tapered waveguide pair as an initial refractive-index distribution and optimize it with lengths of 100, 200, and 500 μm. The widths of the input/output waveguides and tapered waveguide apertures are 7 and 25 μm, respectively. We set the input and desired output fields at the fundamental modes of the input and output waveguides. The calculation steps in the x-axis and z-axis directions were 0.2 and 0.5 μm, respectively. A wavelength of 1550 nm and 40 iterations were used in the calculations. With regard to the mosaic-like pattern approach, we set the minimum core/cladding pixel size at 2×2 μm in consideration of the precision of the fabrication process.

Fig. 3(a) and (b) shows the optimized patterns of waveguide lenses with a length of 500 μm obtained by using the solid pattern and mosaic-like pattern approaches, respectively. A tapered waveguide pair and a constant-width (or straight) waveguide pair are also investigated for comparison [Fig. 3(c) and (d)]. Fig. 4(a) and (b) shows an enlarged view of Fig. 3(a) and (b), respectively. In the mosaic-like pattern [Fig. 4(b)], the interfaces between the core and the cladding are arranged at a location where the optical intensity is high. Consequently, a large amount of light is reflected and vertically scattered at the interfaces, and this results in an excess loss. Thus, we propose the solid pattern approach for suppressing light reflection and vertical scattering. With the solid pattern approach, we restrict the cladding pixel surrounded by the core pixels in the calculation process; this restriction synthesizes solid waveguide shapes. The convergence speed of the proposed approach is slower than that of the mosaic-like pattern approach; however, this restriction can provide optimized waveguides with lower excess loss because the light reflection and the vertical scattering are suppressed. As shown in Fig. 4(a), waveguide lenses designed with the solid pattern approach have aperiodically modulated widths without isolated cladding pixels in the waveguide lens. Fig. 5 shows the result of a BPM simulation of the field propagation in the lens pair optimized using the solid pattern approach, where the wavelength was 1550 nm. As seen in Fig. 5, the input field is focused at the center of the slab region and refocused at the output port. This result indicates that the

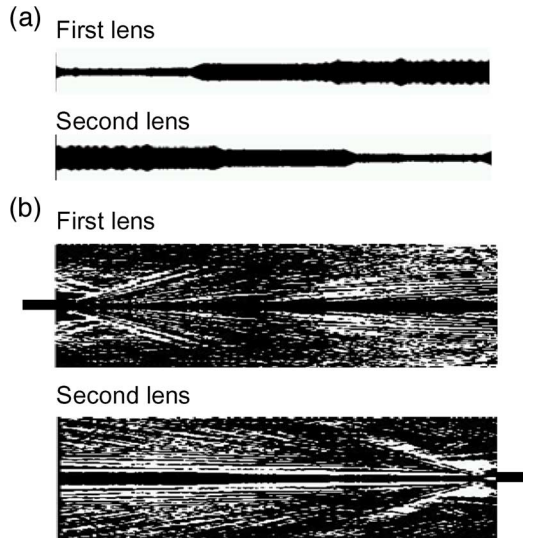

Fig. 4. Enlarged view of waveguide lenses. (a) Solid pattern approach. (b) Mosaic-like pattern approach.

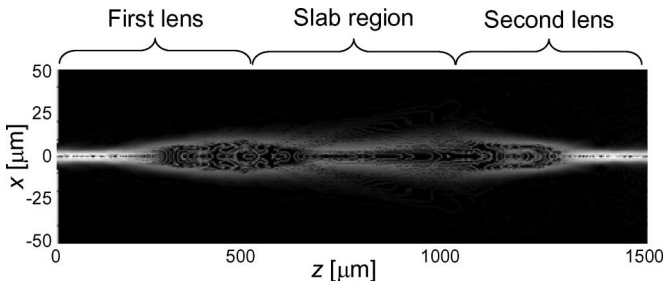

Fig. 5. BPM simulation result of field propagation.

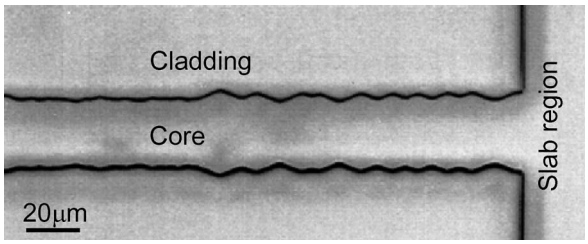

Fig. 6. Optical microscope image of fabricated core pattern.

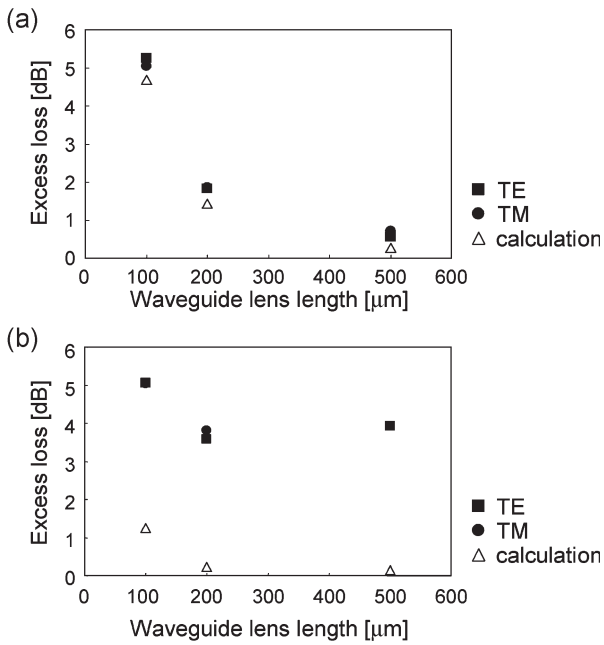

Fig. 7. Express loss of waveguide lens pair. (a) Solid pattern approach. (b) Mosaic-like pattern approach.

wavefront at the output of the waveguide lens is adjusted by aperiodically modulated widths to converge.

We fabricated our designed waveguide lens pairs using silica-based PLC technology [1]. First, undercladding and core glass layers were deposited on a silicon substrate using flame hydrolysis deposition (FHD). The waveguide patterns were then fabricated by photolithography and reactive-ion etching (RIE). After that, the core ridge structures were covered with an overcladding layer again with FHD. Fig. 6 shows the fabricated core pattern observed with an optical microscope before the overcladding layer was fabricated. We ensured that the resolution of the photolithography and RIE processes in our experiments was sufficient for fabricating our designed waveguide patterns. The refractive-index difference between the core and cladding layers was 0.75%, and the core layer was 6 μm thick. We also fabricated a tapered waveguide pair [Fig. 3(c)] and a waveguide pair with a constant width [Fig. 3(d)] as references. The length of the tapered waveguide was set at 2 mm for adiabatic mode conversion, and the width was 25 μm, which was the same as the lens aperture of our designed lenses.

We measured the transmittances of our fabricated waveguide lens pairs. Fig. 7(a) and (b) shows the excess losses of the waveguide lens pair designed by the solid pattern and mosaic-like pattern approaches, respectively, at a wavelength of

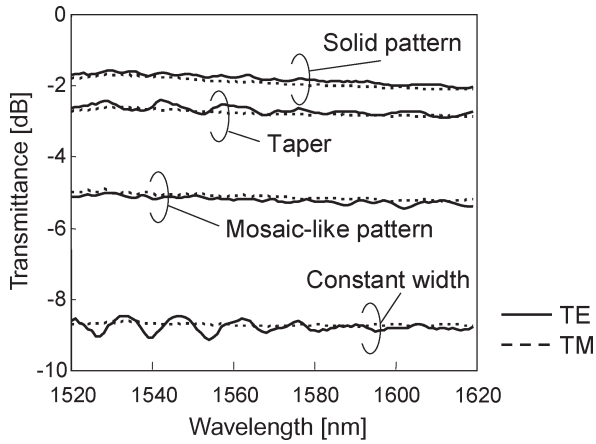

Fig. 8. Measured transmittance of fabricate waveguide lens.

1550 nm. For the solid pattern, the measured excess losses agreed well with the predicted values calculated by BPM. The excess loss decreased as the length of the designed waveguide increased, which indicates that a certain length is required to adjust the wavefront at the output. On the other hand, for the mosaic-like pattern, there was a large discrepancy between the experimental results and the theoretical predictions, and the excess losses were much higher than those of the solid pattern. These results clearly show that the reflection and vertical scattering losses generated in the mosaic-like pattern were suppressed by the solid pattern approach. Fig. 8 shows the measured transmittances of our designed waveguide lens pairs with a length of 500 μm [Fig. 4(a) and (b)] compared with those of tapered [Fig. 4(c)] and constant-width [Fig. 4(d)] waveguides, which include the fiber-coupling losses. The measured loss of the solid pattern was about 6.5 dB lower than that of the constant-width waveguide pair and 1 dB lower than that of the tapered waveguide pair. In addition, the polarization-dependent loss, which mainly results from the excitation of higher order modes, was less than 0.3 dB. This value was lower than those of the tapered and constant-width waveguide pairs. These results indicate that the fabricated waveguides function as a lens, and the solid pattern approach based on the WFM method is useful for designing low-loss waveguide patterns. We think that this type of waveguide lens pair is useful for loss reduction when we incorporate optical bulk components such as thin film filters in PLC devices.

IV. Application to Waveguide Elements

In this section, we describe the application of the solid pattern approach to Y-branches [9] and waveguide crossings [10] and provide detailed experimental results with regard to each element to confirm the practical effectiveness of our proposed approach.

A. Y-Branch Waveguides

A Y-branch waveguide is a fundamental element in PLC devices. For instance, waveguide-type $1 \times N$ splitters consisting of cascaded Y-branches are essential components for optical signal distribution in passive optical network systems [11].

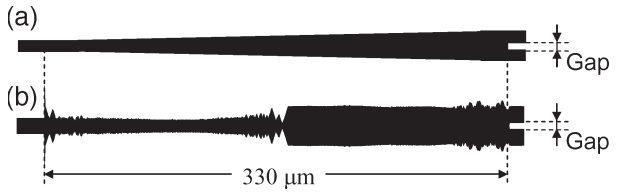

Fig. 9. Y-branch waveguide patterns. (a) Tapered waveguide. (b) Our designed waveguide.

At the same time, Y-branches play important roles as optical signal dividers/combiners in functional PLC devices, such as a differential quadrature phase-shift-keying modulator [12]. The performance improvement and miniaturization of Y-branches are becoming increasingly important in terms of constructing cost-effective access network systems and fabricating compact functional PLC devices with high-density integration.

Fig. 9(a) shows the conventional Y-branch pattern, in which one input port and two output ports are connected via a tapered waveguide. Excess loss, which is a major problem with respect to Y-branches, is caused by the field mismatch at the branching point, namely, the interface between the tapered waveguide and the two output waveguides. This degradation results from the fact that the gap between the two output waveguides cannot be zero because of the limited resolution of the photolithographic and RIE processes. The excess loss becomes more significant for higher refractive-index difference waveguides because the waveguide width decreases, whereas the minimum width of the gap remains constant. As a way of reducing the excess loss resulting from the field mismatch, Wang *et al.* [13] reported a Y-branch with a multimode waveguide transition section, and Gamet and Pandraud [14] introduced a segment design in the branching region.

We designed Y-branches to reduce the excess loss using the solid pattern approach. The input and desired output fields were set at the fundamental mode of the input waveguide and the fundamental local normal mode of the two output waveguides, respectively. The calculation steps in the x-axis and z-axis directions were 0.2 and 0.5 μm, respectively. A wavelength of 1550 nm and 40 iterations were used in the calculations. Fig. 9(b) shows our designed low-loss Y-branch waveguide pattern. The length was 330 μm, and the width and the separation of the access waveguide were 7 and 10 μm, respectively. Note that we set the minimum gap at 3 μm, which is larger than that of commercially available PLC splitters, to accurately compare the excess losses between the WFM design and the tapered waveguide pattern. If the designed waveguide patterns have precipitous spikes, it is difficult to exactly fabricate waveguides as we designed. Thus, we restrict the variation of the waveguide width $\Delta W = W_m - W_{m-1}$, where W_m is the waveguide width at $z = m\Delta z$, to suppress the incidence of spikes. In this study, we limit the maximum value of $|\Delta W|$ to 2 μm in the WFM calculation. Therefore, the optimized pattern has no precipitous spikes, and the waveguide width gradually changes along the z-axis direction. The designed Y-branches were fabricated using silica-based PLC technology. The refractive-index difference was 0.75%, and the core thickness was 6 μm.

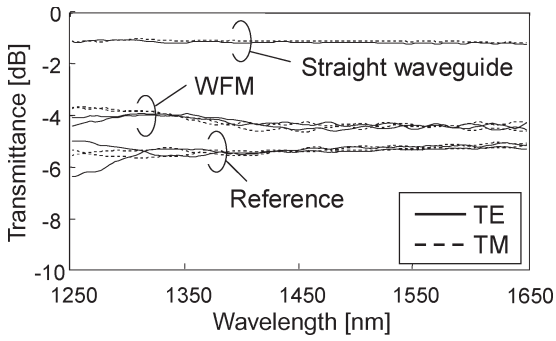

Fig. 10. Measured transmittance of fabricated Y-branch.

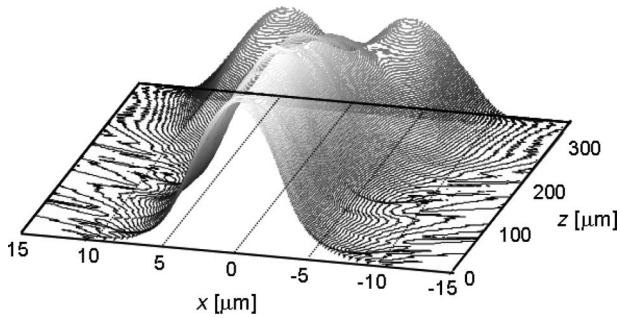

Fig. 11. Waveform transients of the optical power for the WFM designed Y-branch.

Fig. 10 shows the measured transmittance of the fabricated Y-branch waveguides. The excess loss of our designed Y-branch, as determined relative to the straight waveguide on the same chip and the intrinsic 3-dB splitting loss, was 0.2 dB at 1550 nm. This value is about 1 dB lower than that of our reference Y-branch splitter. In addition, the polarization-dependent loss was less than 0.1 dB at 1550 nm. The substantial loss reduction up to 1 dB is attributable to the fact that we set the minimum gap at 3 μm. Although it seems that the advantage of the WFM method decreases when we use a silica waveguide with a gap of less than 3 μm, which can be achieved with the conventional fabrication process, the WFM method has a loss reduction effect even for such narrow gap values [15]. Moreover, we think that even if there is only a slight improvement in one branching point, it will greatly contribute to improving the performance of splitters with a large number of Y-branches in a cascade configuration. Fig. 11 shows the waveform transients of the optical power calculated by using BPM for the WFM-designed Y-branch at a wavelength of 1550 nm. The optimized pattern converts the input field into a double-peak intensity profile at two output waveguides and solves the mode mismatch problem. This is why the excess loss of the Y-branch was substantially reduced by using the WFM method.

B. Waveguide Crossings

Functional PLC devices, such as the arrayed-waveguide grating wavelength multiplexer/demultiplexer with a variable optical attenuator (V-AWG) [16] and the $N \times N$ matrix switch [17], are key components at the nodes of reconfigurable optical add/drop multiplexers and optical cross-connect architectures. Since these devices have a large number of waveguide

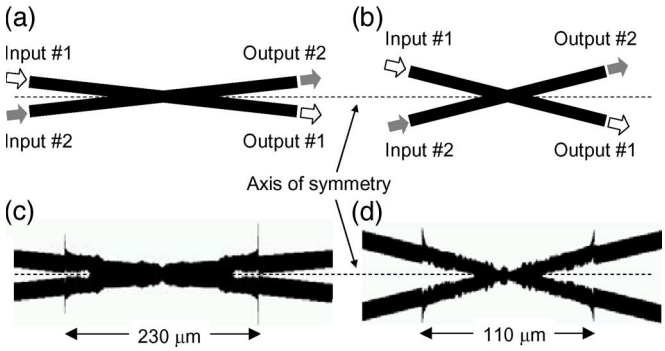

Fig. 12. Waveguide patterns of the reference [(a) 5° and (b) 20°] and our designed [(c) 5° and (d) 20°] crossings.

crossings, their performance is a critical issue in terms of providing higher quality PLC devices. In general, decreasing the crossing angle of waveguide crossings enables us to miniaturize the devices. However, the excess loss and the crosstalk increase as the crossing angle decreases because a considerable amount of incident light couples into another waveguide. Thus, for example, the crossing angle has to be larger than 30° to obtain a loss of less than 0.1 dB and a crosstalk of less than −30 dB in silica waveguides with a 0.75% refractive-index deference. Thus, several methods have been proposed for solving this problem [18]–[20]. In [20], it is reported that crossings with multimode interference coupler structures have a crosstalk value of less than −30 dB, owing to multimode interference. However, the introduction of a multimode waveguide into the waveguide crossing sections reduces the design flexibility because we have to implement an extra region, such as a tapered waveguide, to adiabatically adjust the access waveguide width. Therefore, it remains difficult to achieve a low loss and a low crosstalk for a crossing angle of less than 20°, regardless of the access waveguide width.

We designed waveguide crossings with crossing angles ranging from 5° to 20° using the solid pattern approach. Fig. 12(a) and (b) shows the simple crossing patterns, which are reference crossings in our study, for 5° and 20°, respectively. The input and desired output fields were set at the fundamental modes of input #1 and output #1, respectively. If we optimize the crossings without taking waveguide #2 into account, the input light launched into input #2 will not reach output #2. Thus, we imposed a restriction in the WFM calculation to give the optimized pattern the symmetry as shown in Fig. 12. The parameters used in the calculation, namely, wavelength, iteration, and the maximum value of $|\Delta W|$, were the same as those used for the design of the Y-branches. Waveguides #1 and #2 were both 7 μm wide. Fig. 12(c) and (d) shows the waveguide crossings designed for crossing angles of 5° and 20°. The lengths of the designed regions were 230 and 110 μm, respectively. Fig. 13 shows the measured excess loss and crosstalk of our designed and reference waveguide crossings, which we fabricated with a 0.75% refractive-index difference waveguide, as a function of the crossing angles at 1550 nm. In Fig. 13, the solid and dotted lines show the loss calculated with BPM for our designed pattern and reference waveguide crossings, respectively. The measured excess losses agree well with the BPM simulation

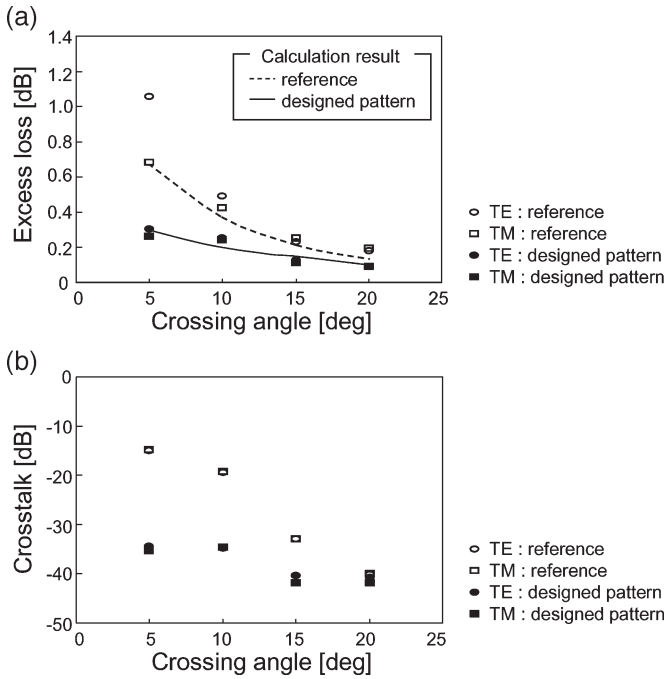

Fig. 13. (a) Excess loss and (b) crosstalk of fabricated waveguide.

result. With a crossing angle of 5°, for example, the excess loss and the crosstalk were reduced from 0.7 to 0.35 dB and from −15 to −35 dB, respectively. This result clearly shows that the performance of the waveguide crossings was substantially improved by using the WFM method.

V. Conclusion

We proposed a new optical waveguide design method, namely, the solid pattern approach based on the WFM method. We designed waveguide lenses, Y-branches, and waveguide crossings by using the solid pattern approach and fabricated them with silica-based PLC technology. We successfully demonstrated that the solid pattern approach is suitable for designing low-loss waveguide devices. We believe that the WFM method with the above approach is useful for improving the optical characteristics and reducing the size of a wide variety of PLC devices.

Appendix

Here, we mathematically prove that the coupling efficiency of an optical circuit (3) is given by the overlap integral between the forward-propagation input field and the backward-propagating desired output field at an arbitrary position (4).

First, we describe the reciprocity of an optical circuit. From the BPM, the optical field φ_M, where φ_0 propagates from $z = 0$ to $z = M\Delta z$, is given by

$$\varphi_M = \mathbf{H}_M \cdots \mathbf{H}_m \cdots \mathbf{H}_1 \varphi_0 \tag{8}$$

where $\mathbf{A}\mathbf{B}_m\mathbf{A}$ is rewritten as $\mathbf{H}_m$ for brevity. Then, we consider the Hermitian conjugate of (8), i.e.,

$${}^t\varphi_M^* = {}^t(\mathbf{H}_M \cdots \mathbf{H}_m \cdots \mathbf{H}_1 \varphi_0)^* \tag{9}$$

where $\mathbf{H}_m^*$ and ${}^t\mathbf{H}_m$ denote the complex conjugate and transposed matrix of $\mathbf{H}_m$, respectively. According to the property of the Hermitian conjugate, (9) can be transformed as follows:

$$ {}^t\varphi_M^* = {}^t\varphi_0^* \, {}^t\mathbf{H}_1^* \cdots {}^t\mathbf{H}_m^* \cdots {}^t\mathbf{H}_M^*. \tag{10} $$

Since $\mathbf{H}_m$ has the unity and symmetry for a lossless waveguide, the following equations are approved:

$$ {}^t\mathbf{H}_m^* = \mathbf{H}_m^{-1} \quad \text{and} \quad {}^t\mathbf{H}_m = \mathbf{H}_m \tag{11} $$

where $\mathbf{H}_m^{-1}$ denotes the inverse matrix of $\mathbf{H}_m$. Therefore, (10) is transformed using (11) as follows:

$$ {}^t\varphi_M^* \mathbf{H}_M \cdots \mathbf{H}_m \cdots \mathbf{H}_1 = {}^t\varphi_0^*. \tag{12} $$

Then, when we consider the transposed matrix of both sides of (12), the following equation is derived from (11):

$$ \mathbf{H}_1 \cdots \mathbf{H}_m \cdots \mathbf{H}_M \varphi_M^* = \varphi_0^*. \tag{13} $$

Equation (13) means that if φ_M^* enters an optical circuit from $z = M\Delta z$, the propagation field at $z = 0$ is equivalent to φ_0^*, that is, the reciprocity of an optical circuit. Note that the complex conjugate means that the propagation axis is reversed.

Next, we look at the coupling coefficient η of an optical circuit. When we consider the output field $\phi_M(x)$ and desired output field $\psi_M(x)$ to be a matrix, the coupling coefficient η is given by

$$ \begin{aligned} \eta &= \left| \int \psi_M^*(x) \phi_M(x) dx \right|^2 \\ &= \left| \sum {}^t\psi_M^* \phi_M \right|^2 \\ &= \left| \sum {}^t\psi_M^* \mathbf{H}_M \cdots \mathbf{H}_m \cdots \mathbf{H}_1 \phi_0 \right|^2. \end{aligned} \tag{14} $$

Therefore, η can be transformed using (12) as follows:

$$ \begin{aligned} \eta &= \left| \sum \left({}^t\psi_M^* \mathbf{H}_M \cdots \mathbf{H}_{m+1} \right) \left(\mathbf{H}_m \cdots \mathbf{H}_1 \phi_0 \right) \right|^2 \\ &= \left| \sum {}^t\psi_m^* \phi_m \right|^2 \\ &= \left| \int \psi_m^*(x) \phi_m(x) dx \right|^2. \end{aligned} \tag{15} $$

This equation means that if an optical circuit has reciprocity, the coupling efficiency is given by the overlap integral between the forward-propagating input field and the backward-propagating desired output field at an arbitrary position $z = m\Delta z$.

ACKNOWLEDGMENT

The authors would like to thank T. Kitagawa, S. Suzuki, T. Ooyama, I. Ogawa, T. Kitoh, Y. Hida, M. Kohtoku, and Y. Inoue for valuable discussions and their continuous support.

REFERENCES

[1] A. Himeno, K. Kato, and T. Miya, "Silica-based planar lightwave circuits," *IEEE J. Sel. Topics Quantum Electron.*, vol. 4, no. 6, pp. 913–924, Nov./Dec. 1998.

[2] M. M. Spuhler, B. J. Offrein, G. L. Bona, R. Germann, I. Massarek, and D. Erni, "A very short planar silica spot-size converter using a nonperiodic segmented waveguide," *J. Lightw. Technol.*, vol. 16, no. 9, pp. 1680–1685, Sep. 1998.

[3] T. Yabu, M. Geshiro, and S. Sawa, "New design method for low-loss Y-branch waveguides," *J. Lightw. Technol.*, vol. 19, no. 9, pp. 1376–1384, Sep. 2001.

[4] D. Correia, J. P. da Silva, and H. E. Hernandez-Figueroa, "Genetic algorithm and finite-element design of short single-section passive polarization converter," *IEEE Photon. Technol. Lett.*, vol. 15, no. 7, pp. 915–917, Jul. 2003.

[5] B. Luyssaert, P. Bienstman, P. Vandersteegen, P. Dumon, and R. Baets, "Efficient nonadiabatic planar waveguide tapers," *J. Lightw. Technol.*, vol. 23, no. 8, pp. 2462–2468, Aug. 2005.

[6] M. Yang, H. Chen, K. J. Webb, S. Minin, S. L. Chuang, and G. R. Cueva, "Demonstration of mode conversion in an irregular waveguide," *Opt. Lett.*, vol. 31, no. 3, pp. 383–385, Feb. 2006.

[7] T. Hashimoto, T. Saida, I. Ogawa, M. Kohtoku, T. Shibata, and H. Takahashi, "Optical circuit design based on a wavefront-matching method," *Opt. Lett.*, vol. 30, no. 19, pp. 2560–2562, Oct. 2005.

[8] T. Saida, T. Hashimoto, I. Ogawa, M. Kohtoku, T. Shibata, H. Takahashi, and S. Suzuki, "Fabrication of wavelength splitter designed by wavefront matching method," presented at the Optical Fiber Commun. Conf. (OFC), Anaheim, CA, 2005, Paper OThV2.

[9] Y. Sakamaki, T. Saida, T. Shibata, Y. Hida, T. Hashimoto, M. Tamura, and H. Takahashi, "Y-branch waveguides with stabilized splitting ratio designed by wavefront matching method," *IEEE Photon. Technol. Lett.*, vol. 18, no. 7, pp. 817–819, Apr. 2006.

[10] Y. Sakamaki, T. Saida, M. Tamura, T. Hashimoto, and H. Takahashi, "Low loss and low crosstalk waveguide crossings designed by wavefront matching method," *IEEE Photon. Technol. Lett.*, vol. 18, no. 19, pp. 2005–2007, Oct. 2006.

[11] H. Ueda, K. Okada, B. Ford, G. Mahony, S. Hornung, D. Faulkner, J. Abiven, S. Durel, R. Ballart, and J. Erickson, "Deployment status and common technical specifications for a B-PON system," *IEEE Commun. Mag.*, vol. 39, no. 12, pp. 134–141, Dec. 2001.

[12] T. Yamada, Y. Sakamaki, T. Saida, A. Kaneko, A. Sano, and Y. Miyamoto, "86-Gb/s differential quadrature phase-shift-keying modulator using hybrid assembly technique with planar lightwave circuit and $LiNbO_3$ devices," in *Proc. LEOS*, Montreal, QC, Canada, 2006, pp. 963–964.

[13] Q. Wang, S. He, and L. Wang, "A low-loss Y-branch with a multimode waveguide transition section," *IEEE Photon. Technol. Lett.*, vol. 14, no. 8, pp. 1124–1126, Aug. 2002.

[14] J. Gamet and G. Pandraud, "Ultralow-loss 1×8 splitter based on field matching Y junction," *IEEE Photon. Technol. Lett.*, vol. 16, no. 9, pp. 2060–2062, Sep. 2004.

[15] Y. Sakamaki, T. Saida, M. Tamura, T. Hashimoto, and H. Takahashi, "Low-loss Y-branch waveguides designed by wavefront matching method and their application to a compact 1×32 splitter," *Electron Lett.*, vol. 43, no. 4, pp. 217–219, Feb. 2007.

[16] A. Kaneko, Y. Doi, Y. Hashizume, S. Kamei, Y. Tamura, I. Ogawa, T. Kominato, and S. Suzuki, "Ultra small 16ch variable optical attenuator multiplexer (V-AWG) using multi-chip PLC integration technology for ROADM," in *Proc. ECOC*, Glasgow, U.K., 2005, pp. 987–990.

[17] T. Goh, M. Yasu, K. Hattori, A. Himeno, M. Okuno, and Y. Ohmori, "Low loss and high extinction ratio strictly nonblocking 16×16 thermooptic matrix switch on 6-in wafer using silica-based planar lightwave circuit technology," *J. Lightw. Technol.*, vol. 19, no. 3, pp. 371–379, Mar. 2001.

[18] K. Aretz and H. Bulow, "Reduction of crosstalk and losses of intersecting waveguide," *Electron. Lett.*, vol. 25, no. 11, pp. 730–731, May 1989.

[19] M. G. Daly, P. E. Jessop, and D. Yevick, "Crosstalk reduction in intersecting rib waveguides," *J. Lightw. Technol.*, vol. 14, no. 7, pp. 1695–1698, Jul. 1996.

[20] G. Przyrembel and B. Kuhlow, "Waveguide crossings with low crosstalk at small angles," *Electron. Lett.*, vol. 38, no. 24, pp. 1533–1535, Nov. 2002.

Yohei Sakamaki (M'05) was born in Japan in 1979. He received the B.S. and M.S. degrees in material science and engineering from Kyoto University, Kyoto, Japan, in 2002 and 2004, respectively.

Since joining Nippon Telegraph and Telephone Photonics Laboratories, Atsugi, Japan, in 2004, he has been engaged in research on optical waveguide design using the wavefront matching method.

Mr. Sakamaki is a member of the Institute of Electronics, Information, and Communication Engineers of Japan and the IEEE Laser and Electro-Optics Society.

Takashi Saida (M'99) was born in Yamaguchi, Japan, in 1969. He received the B.S., M.S., and Ph.D. degrees in electrical engineering from Tokyo University, Tokyo, Japan, in 1993, 1995, and 1998, respectively.

From 1996 to 1998, he was with Japan Society for the Promotion of Science as a Research Fellow. In 1998, he joined Nippon Telegraph and Telephone (NTT) Corporation, Ibaraki, Japan, where he was engaged in the research and development on functional silica-based planar lightwave circuits (PLCs). From 2002 to 2003, he was a Visiting Scholar at Stanford University, Stanford, CA, on leave from NTT Laboratories. In 2006, he joined NTT Electronics Corporation, Ibaraki, and is the Director of design group at PLC business unit.

Dr. Saida is a member of the Optical Society of America, the Institute of Electronics, Information, and Communication Engineers of Japan, and the Japan Society of Applied Physics.

Toshikazu Hashimoto received the B.S. and M.S. degrees in physics from Hokkaido University, Sapporo, Hokkaido, Japan, in 1991 and 1993, respectively.

In 1993, he joined Nippon Telegraph and Telephone Photonics Laboratories, Japan. He has been engaged in research on hybrid integration technology using planar lightwave circuits and the wavefront matching method.

Mr. Hashimoto is a member of the Institute of Electronics, Information, and Communication Engineers of Japan and the Physical Society of Japan.

Hiroshi Takahashi (M'92) was born in Japan in 1963. He received the B.S. and M.S. degrees in electrical engineering and the Ph.D. degree from Tohoku University, Aoba, Japan, in 1986, 1988, and 1997, respectively.

In 1988, he joined Nippon Telegraph and Telephone (NTT) Laboratories, where he was engaged in research on the design and fabrication of silica-based optical waveguide devices including arrayed waveguide grating (AWG) wavelength multiplexers/demultiplexers.

From 1998 to 2001, he was with NTT Electronics, where he developed the first AWG multiplexer/demultiplexer for commercial DWDM systems. He is currently a Research Group Leader with NTT Photonics Laboratories, Atsugi, Japan, where he is working on a new optical waveguide design based on the wavefront matching method and various kinds of waveguide circuits such as AWGs, Mach–Zehnder interferometer-based switches, reconfigurable optical add/drop multiplexing modules, dispersion compensators, and optical filters/discriminators for advanced modulations including phase shift keying and code division multiplexing.

Dr. Takahashi is a member of the Institute of Electronics, Information, and Communication Engineers of Japan, the Japan Society of Applied Physics, and the IEEE Laser and Electro-Optics Society.